

31. D'Argenio DZ, Schumitzky A. A program package for simulation and parameter estimation in pharmacokinetic systems. *Comput Prog Biomed* 1979;9:115-134.
32. Odom-Maryon TL, Chai A, Williams LE, et al. Pharmacokinetics and modeling of cT84.66 chimeric anti-CEA antibody in humans. *J Nucl Med*; in press.
33. Loevinger R, Berman M. MIRD Pamphlet No. 1, Revised. New York: Society of Nuclear Medicine; 1976.
34. Stabin MG. MIRDOSE: personal computer software for internal dose assessment in nuclear medicine. *J Nucl Med* 1996;37:538-546.
35. Siegel JA, Wessels BW, Watson EE, et al. Bone marrow dosimetry and toxicity for radioimmunotherapy. *Antibody Immunocnj Radiopharm* 1990;3:213-233.
36. Buras RB, Williams LE, Beatty BG, Wong JYC, Beatty JD, Wanek PM. A method including edge effects for the estimation of radioimmunotherapy absorbed doses in the tumor xenograft model. *Med Phys* 1994;21:287-292.
37. Corbisiero RM, Yamauchi DM, Williams LE, et al. Comparison of immunoscintigraphy and computerized tomography in identifying colorectal cancer: individual lesion analysis. *Cancer Res* 1991;51:5704-5711.
38. Patt YZ, Lamki LM, Haynie TP, et al. Improved tumor localization with increasing dose of indium-111-labeled anti-carcinoembryonic antigen monoclonal antibody ZCE-025 in metastatic colorectal cancer. *J Clin Oncol* 1988;8:1220-1230.
39. Patt YZ, Lamki LM, Shanken J, et al. Imaging with indium-111-labeled anticarcinoembryonic antigen monoclonal antibody ZCE-025 of recurrent colorectal or carcinoembryonic antigen-producing cancer in patients with rising serum carcinoembryonic antigen levels and occult metastases. *J Clin Oncol* 1990;8:1246-1254.
40. Yu B, Carrasquillo J, Milenic D, et al. Phase I trial of iodine 131-labeled COL-1 in patients with gastrointestinal malignancies: influence of serum carcinoembryonic antigen and tumor bulk on pharmacokinetics. *J Clin Oncol* 1996;6:1798-1809.
41. Beatty BG, Beatty JD, Williams LE, Paxton RJ, Shively JE, O'Connor-Tressel M. Effect of specific antibody pretreatment on liver uptake of <sup>111</sup>In-labeled anticarcinoembryonic antigen monoclonal antibody in nude mice bearing human colon cancer xenografts. *Cancer Res* 1989;49:1587-1594.
42. Williams LE, Beatty BG, Beatty JD, Wong JYC, Paxton RJ, Shively JE. Estimation of monoclonal antibody-associated <sup>90</sup>Y activity needed to achieve certain tumor radiation doses in colorectal cancer patients. *Cancer Res* 1990;50(suppl):1029s-1030s.
43. Weiden PL, Breitz HB, Seiler CA, et al. Rhenium-186-labeled chimeric antibody NR-LU-13: pharmacokinetics, biodistribution and immunogenicity relative to murine analog NR-LU-10. *J Nucl Med* 1993;34:2111-2119.
44. Williams LE, Duda RB, Proffitt RT, et al. Tumor uptake as a function of tumor mass: a mathematical model. *J Nucl Med* 1988;29:103-109.
45. Kuhn JA, Corbisiero RM, Buras RR, et al. Intraoperative gamma detection probe with presurgical antibody imaging in colorectal cancer. *Arch Surg* 1991;126:1398-1403.
46. Epenetos AA. Antibody guided lymphangiography in the staging of cervical cancer. *Br J Cancer* 1985;51:805-808.
47. Cote RJ, Houchens DP, Hitchcock CL, et al. Intraoperative detection of occult colon cancer micrometastases using <sup>125</sup>I-radiolabeled monoclonal antibody CC49. *Cancer* 1996;77:613-620.

# Pharmacokinetic Modeling and Absorbed Dose Estimation for Chimeric Anti-CEA Antibody in Humans

Tamara L. Odom-Maryon, Lawrence E. Williams, Akiko Chai, George Lopatin, An Liu, Jeffrey Y.C. Wong, Jeffrey Chou, Kenneth G. Clarke and Andrew A. Raubitschek  
*Departments of Biostatistics and Radioimmunotherapy and Divisions of Radiology and Radiation Oncology, City of Hope National Medical Center, Duarte, California, and Department of Radiological Sciences, University of California at Los Angeles Medical Center, Los Angeles, California*

The objective of this article was to model pharmacokinetic data from clinical diagnostic studies involving the <sup>111</sup>In-labeled monoclonal antibody (MAb) chimeric T84.66, against carcinoembryonic antigen. Model-derived results based on the <sup>111</sup>In-MAb blood, urine and digital imaging data were used to predict <sup>90</sup>Y-MAb absorbed radiation doses and to guide treatment planning for future therapy trials. Fifteen patients with at least one carcinoembryonic antigen-positive lesion were evaluated. We report the kinetic parameter estimates and absorbed <sup>111</sup>In-MAb dose and projected <sup>90</sup>Y-MAb doses for each patient as well as describe our approach and rationale for modeling an extensive set of pharmacokinetic data. **Methods:** The ADAPT II software package was used to create three- and five-compartment models of uptake against time in the patient population. The "best-fit" model was identified using ordinary least squares. Areas under the curve were calculated using the modeled curves and input into MIRDOSE3 to estimate absorbed radiation doses for each patient. **Results:** A five-compartment model best described the liver, whole body, blood and urine data for a subcohort of nine patients with digital imaging data. A three-compartment model best described the blood and urine data for all 15 clinical patients accrued in the clinical trial. For the subcohort, the largest projected <sup>90</sup>Y-MAb doses were delivered to the liver (mean, 24.78 rad/mCi; range, 15.02-37.07 rad/mCi), with red marrow estimates on the order of 3.32 rad/mCi (range, 1.24-5.55) of <sup>90</sup>Y. Corresponding estimates for the <sup>111</sup>In-MAb were 3.18 (range, 2.09-4.43) and 0.55 (range, 0.34-0.74), respectively. **Conclusion:** The three- and five-compartment models presented here were successfully used to represent the blood, urine and imaging data. This was evidenced by the small standard errors for the kinetic parameter estimates and R<sup>2</sup> values close to 1. As planned future therapeutic trials will involve stem cell support to alleviate hematological toxicities, the develop-

ment of an approach for estimating doses to other major organs is crucial.

**Key Words:** compartmental models; anti-CEA; chimeric antibody; dose estimation

**J Nucl Med 1997; 38:1959-1966**

**M**onoclonal antibodies (MAbs) have had multiple clinical applications in both diagnostic (1-3) and therapeutic (4-6) nuclear medicine. Originally, most of these agents were murine antibodies generated by injecting normal mice with human tumor cells or other human proteins of interest. In the case of serial studies in the same patient, however, the use of such murine antibodies has typically led to the induction of a human antimouse antibody response (7,8). Others have suggested that the use of chimeric antibodies should reduce the incidence of human antiprotein responses (9,10). In this strategy, two-thirds of the murine IgG molecule is replaced with the corresponding human sequences by using recombinant DNA technology. Because the patient is less likely to develop a human antichimeric antibody response, the potential for serial therapeutic infusions is increased. As the use of chimeric molecules could result in changes in the human pharmacokinetics (PK), determination of a mathematical model describing the biodistribution of the antibody in the human system is desirable. Molecular changes in the MAb could then be correlated with variations in the model parameter estimates.

Although mathematical modeling has had a long association with the study of radiotracers (11), the application of modeling in clinical studies of antibodies has been much less extensive (9,10,12). A fundamental goal of such analyses is to establish a set of parameters that describe the distribution of a radiolabeled

Received Apr. 18, 1996; revision accepted Dec. 10, 1996.

For correspondence or reprints contact: Tamara L. Odom-Maryon, PhD, Department of Biostatistics, City of Hope, 1500 E. Duarte Rd, Duarte, CA 91010.

**TABLE 1**  
Schedule of Data Acquisition Times for 15 Patients Enrolled in the Chimeric T84.66 Clinical Diagnostic Study

Data source	Planned collection times post-antibody infusion	Median (range)
Blood*	Start of infusion, 30 min, 1, 2 and 6 hr and every imaging scan time	8 samples (7–9 samples)
Urine	Daily urine collections for up to 5 days postinfusion (collected by the patient)	Last collection, 83 hr (60–155 hr)
Images		
spot/whole body	6, 24, and 48 hr, one scan between 4 and 7 days	Last scan, 132 hr (73–259 hr)
SPECT†	48 hr, one scan between 4 and 7 days	Last scan, 115 hr (44–168 hr)

\*In addition to the times listed in the table, several blood samples may have been drawn during the first 30 min following infusion. After 12 patients were accrued to the trial, the blood specimen collection times were changed to the start of infusion and 4, 16, 36, 38, 108, 168 and 500 hr postinfusion.

†All 15 patients underwent gamma camera imaging; however, digitally stored imaging data were only available for the last 9 eligible and evaluable patients accrued to the trial.

material in humans. Through modeling, the area under the curve (AUC) of activity against time is determined and used in the estimation of absorbed radiation doses to normal organs and tumors. For trials involving an initial infusion of an antibody labeled with an imaging isotope followed by an infusion with a therapeutic isotope (beta-emitter), model-derived results based on the imaging infusion can be used to predict the behavior of the therapeutic labeled antibody and, therefore, guide treatment planning. Parameter estimates based on a model incorporating data from several organs (blood, urine, whole body and liver) rather than that of a single organ are preferred in the determination of the AUC. General multicompartment models are used, with the compartments related to each other through a set of differential equations.

The objective of this article is to model the PK data from a pretherapy pilot imaging trial involving the <sup>111</sup>In-labeled anti-carcinoembryonic antigen (CEA) antibody, chimeric T84.66 (cT84.66). Presence of CEA has been found on a majority of colorectal tumors (13) and other common tumors, including those of the lung (14) and breast (15). The purpose of the imaging trial was to demonstrate the potential usefulness of the cT84.66 antibody as a therapeutic agent when labeled with <sup>90</sup>Y by evaluating the tumor-targeting properties, biodistribution, immunogenicity and PKs of this <sup>111</sup>In-MAb.

## MATERIALS AND METHODS

Materials and methods specific to the molecular engineering, production and characteristics of cT84.66 antibody, as well as the specific aims, eligibility criteria, patient characteristics and clinical findings of our trial, are described in detail in the associated report of Wong et al. (16). In brief, cT84.66 is an intact IgG<sub>1</sub> antibody derived from the murine T84.66 MAb developed at the City of Hope National Medical Center with high specificity and affinity for CEA, and it was genetically engineered to contain the human kappa and gamma constant regions. Purified antibody was conjugated to the isothiocyanatobenzyl diethylenetriaminepentaacetic acid chelate with the immunoreactivity of the conjugate over 95% by solid-phase CEA radioimmunoassay.

Eight men and seven women (median age 62 yr; range 36–72 yr) who had evidence of CEA-producing metastatic disease, based on an elevated serum CEA or positive staining on CEA immunohistochemistry of tumor biopsies, were eligible for the study. All patients had adequate renal and hepatic function before antibody infusion. The antibody was radiolabeled at a ratio of 5 mCi of <sup>111</sup>In to 5 mg of protein and was administered at a rate of 2 ml per min, so as to deliver the entire dose over approximately 25 min.

Table 1 summarizes the scheduled and actual collection times relative to the start of infusion for blood, urine and image sampling.

All patients underwent four serial imaging sessions and, if clinically indicated, also underwent planned surgical exploration within 2 wk after antibody infusion. To reduce fecal gastrointestinal activity, a bowel cathartic was administered to patients before each scan, unless it was felt that the patient could not tolerate such preparation. Blood and urine samples were assayed for <sup>111</sup>In activity by gamma counter. Digital imaging data were available for the last nine patients accrued to the trial (hereafter referred to as the subcohort), making whole-body and normal organ absorbed radiation dose estimates possible from serial <sup>111</sup>In scans. Although the first six consecutive patients accrued to this trial underwent serial imaging sessions, digital images were not captured for these patients. Patients collected their own urine in 24-hr samples; feces were not collected.

## Modeling Strategy

Several compartmental models were fit to each patient's <sup>111</sup>In-MAb. Initial models examined included compartments for the blood and urine data only, and then these were expanded to include compartments for the liver and total body activity. The derivation for the models tested was based on the physiologic principles believed to characterize the distribution of the <sup>111</sup>In-MAb in humans. Initially, all models were fit to a subset of three patients for whom all data were available. Those models demonstrating reasonable fits to the blood, urine, liver and total body data were then tried for all patients.

Estimation of the compartmental model parameters was performed by nonlinear weighted least squares regression using the ADAPT II software package (17) and corroborated using SAAM (11). By standardizing the starting values and convergence criteria used for the two programs, all of the parameter estimates generated using SAAM consistently fell within the 95% confidence interval for the parameter estimates obtained using the ADAPT II software. To determine the best-fitting models, the following criteria were used:

1. For comparing nested models, in which one model was a subset of the larger model, selection of the final model was based on minimization of the estimator criterion value provided in the ADAPT II output and comparison of the Akaike Information Criterion using an F-test (18) and R<sup>2</sup> statistics.
2. To compare two models, neither of which was a subset of the other, the residual sums of squares and R<sup>2</sup> statistics were used.

Urine data were expressed as the cumulative amount voided post-<sup>111</sup>In-MAb infusion. Blood and urine counts were <sup>111</sup>In decay-corrected to the time of sampling and expressed as the

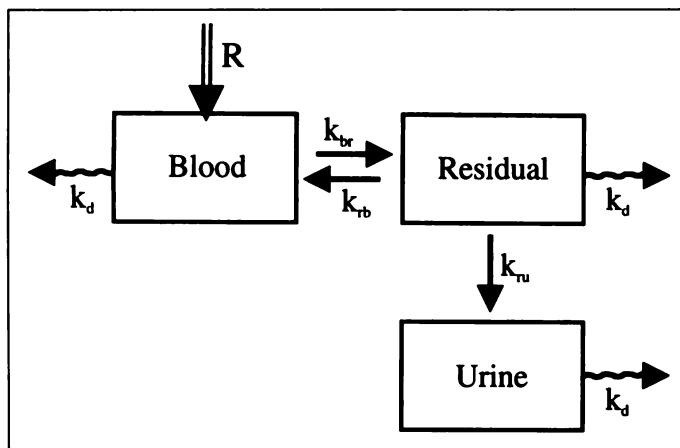


**FIGURE 1.** Three-compartment model (model 3C) used to represent 15 patients receiving  $^{111}\text{In}$ -cT84.66 who had blood and urine data available for analysis. The  $k_d$  arrow symbolizes radiodecay of the radiolabel.

fractional injected activity (IA). A fixed rate constant ( $k_d$ ) representing the physical decay of the radionuclide  $^{111}\text{In}$  was explicitly included in the system of differential equations because of this IA formulation (19). To account for the fact that the MAb was distributed into an unknown volume that was primarily plasma, a parameter ( $V$ ) was also fit to the blood data. Organ and whole-body uptakes were obtained using the geometric mean of the anterior and posterior images, when possible. Regions of interest were drawn around relevant organs to obtain total counts, which were also expressed as the fractional IA (20).

### Weighting Schemes

Several weighting schemes were examined (17), including:

1. Use of weights proportional to the inverse of the data or the inverse of the data squared; and
2. Weights specified by assuming a linear relationship between the data and its variance, then using the maximum likelihood estimation algorithm to estimate the kinetic parameters.

We also evaluated a power function relationship between the variance and the mean response (21); however, this resulted in overparameterization of the data. As the best-fit models based on the  $R^2$  statistics were obtained using unity weights, final parameter estimates for each patient were obtained using ordinary least squares.

### Initial Estimates

For the first analysis, initial values were chosen based on prior experience. Because the Nelder-Mead simplex algorithm used by

ADAPT can be sensitive to poor choices for the initial starting values of model parameters, each patient's data were analyzed using a minimum of two different sets of starting values with the final estimates from each set of starting values being used as new starting values and repeating this process four times. The SAAM package was used to confirm that the results obtained using the ADAPT II software were independent of the convergence algorithm applied.

### Imaging Data

For the modeled organs (whole body, blood and liver), model parameters were used to determine the AUC values by numerical integration of the differential equations. Several organs that were not modeled were sometimes observable in patient images. Spleen and kidneys were occasionally seen; likewise, the heart appeared at very early time points. If visualized, a trapezoidal representation of the data was made to determine the associated AUC. In all cases, the estimates of the AUCs were based on data that were not corrected for radioactive decay (i.e., in units of IA). Estimates of AUCs for the  $^{90}\text{Y}$ -cT84.66 MAb were made by exchanging the physical decay constant of  $^{111}\text{In}$  with that of  $^{90}\text{Y}$  in the modeling equations and calculating the integrals as indicated above.

### Determination of Absorbed Dose Estimates

After the MIRDO formalism (22), organ activity AUCs, in units of mCi-hr, were entered as cumulative activity into the MIRDOSE3 program (23), as provided by the Oak Ridge Associated Universities. In the case of the liver, the source organ AUC was the sum of liver and hepatic blood AUCs, as there is no present provision for blood as a separate source term in the MIRDOSE3 program. As recommended by the AAPM Task Group on Radionuclide Dosimetry, the specific activity for the red marrow was calculated as 0.3 times the blood specific activity determined by the model (24). Total blood mass was estimated with a standard algorithm based on patient mass and height (25). All tumor dose estimates used a single uptake against time curve, determined by serial images from one patient. Doses were estimated by integrating the point source function over the tumor volume determined from pathology specimens when available.

### RESULTS

The final three-compartment model (model 3C) applied to the data from the full cohort is shown in Figure 1, and the final five-compartment model (model 5C) fit to the subcohort is shown in Figure 2. For both models, blood served as the central compartment with a single rate input. The blood pool input function was adjusted to be the constant rate acceptable to a given patient by using a shielded injector device developed at our institution (26). If other inputs occurred as a result of patient

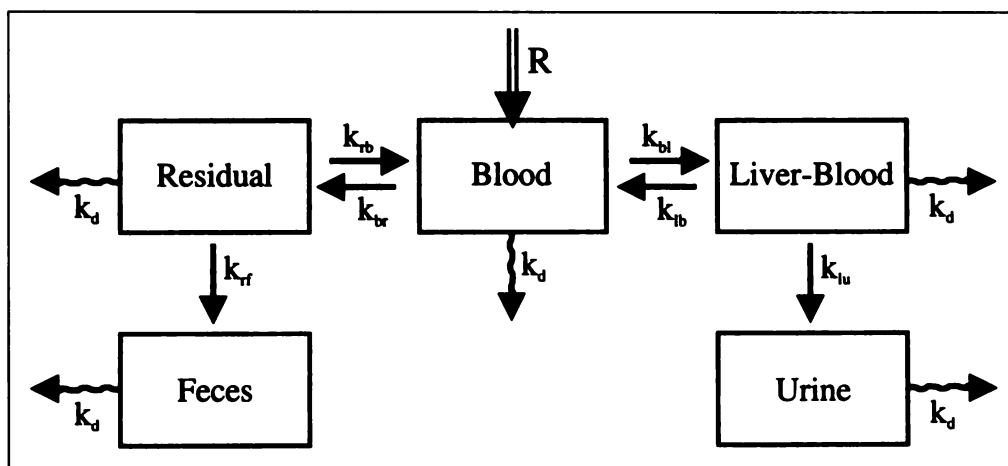


**FIGURE 2.** Five-compartment model (model 5C) of the biodistribution of the  $^{111}\text{In}$ -labeled anti-CEA antibody cT84.66. The  $k_d$  arrow symbolizes radiodecay of the radiolabel. Compartment two consisted of liver and hepatic blood. This model was used to represent nine patients who had digital imaging data.

**TABLE 2**  
Pharmacokinetic Parameter Estimates Based on a Three-Compartment Model Fit to Blood, Urine and Imaging Data from Clinical Diagnostic Studies Involving cT84.66 Labeled with Indium-111

Parameter estimate (s.d.)*	Patient no.															Mean†	s.e.‡	
	1	2	3	4	5	6	7	8	10	11	13	14	15	17	18			
$k_{br}$ (blood to residual; $hr^{-1}$ )	0.403 (0.069)	0.014 (0.004)	0.021 (0.012)	0.001 (0.063)	0.083 (0.004)	0.015 (0.006)	0.030 (0.005)	0.024 (0.005)	0.020 (0.005)	0.027 (0.012)	0.110 (0.002)	0.008 (0.002)	0.074 (0.011)	0.024 (0.006)	0.020 (0.002)	0.064 (0.014)§	0.026	
$K_{rb}$ (residual to blood; $hr^{-1}$ )	0.006 (0.019)	0.007 (0.009)	0.001 (0.005)	0.000 (0.029)	0.007 (0.002)	0.005 (0.017)	0.005 (0.005)	0.012 (0.007)	0.006 (0.002)	0.018 (0.009)	0.000 (0.005)	0.002 (0.005)	0.012 (0.005)	0.010 (0.008)	0.010 (0.004)	0.006 (0.009)	0.001	
$k_{ru}$ (residual to urine; $hr^{-1}$ )	0.005 (0.001)	0.004 (0.001)	0.013 (0.000)	0.003 (0.001)	0.002 (0.000)	0.002 (0.001)	0.002 (0.001)	0.002 (0.000)	0.001 (0.000)	0.002 (0.000)	0.002 (0.000)	0.002 (0.000)	0.002 (0.000)	0.017 (0.000)	0.013 (0.000)	0.002 (0.000)	0.002 (0.000)	0.000
Volume (liters)	6.418 (0.356)	7.540 (0.163)	6.209 (0.108)	6.462 (0.990)	4.770 (0.040)	6.982 (0.207)	8.651 (0.125)	5.290 (0.117)	5.033 (0.032)	4.479 (0.078)	3.822 (0.102)	4.026 (0.067)	4.863 (0.133)	5.089 (0.139)	7.739 (0.103)	5.825 (0.184)	0.374	

\*Parameter estimates and corresponding s.d. obtained using ordinary least squares fit to each patient's data as a function of time.

†Mean parameter estimates obtained by averaging across the 15 patients.

‡s.d. of the mean parameter estimates.

§Average s.d. obtained by averaging across the 15 patients.

responses, the adjusted infusion rate was entered into the analyses. For model 5C, the remaining four compartments included liver, residual body, urine and fecal excretion. Five important features of this model were:

1. Residual activity was included in the model and was constrained to be equal to the difference between the total body activity and the sum of the blood and liver activity.
2. Fecal activity was also included as a separate compartment and was constrained to be equal to the difference between the administered activity and the sum of the urine and total body activity (i.e., fecal data were not directly sampled).
3. Whole-body data were normalized to the first whole-body scan taken immediately after infusion.
4. The image of the liver was considered to contain both liver and blood pool activity, so that one of the fitted parameters ( $f_{bl}$ ) was the fraction ( $<1$ ) of the activity in the hepatic image assigned to the blood pool in the organ.

5. The urine compartment was linked to the liver rather than to a renal compartment.

Because little or no kidney activity was observed in the subcohort, this structure was reasonable. In addition, the radioactive species measured in the urine had a much lower molecular weight (5 kDa) than that found in the blood (160 kDa) and was therefore thought to be the result of a hepatic metabolic process. More details of this feature are presented in the companion paper by Wong et al. (16).

Parameter estimates and corresponding s.d. based on models 3C and 5C are listed in Tables 2 and 3, respectively. In addition, mean parameter estimates, mean s.d. across patients and the s.e. of the mean parameter estimates are reported. To quantify the fit of the two models to the data, the  $R^2$  statistics from each data source and for all patients are shown in Table 4. Using model 3C for all patients, the s.d. for 53 of the 60 parameters estimated (four parameters per patient) were at least two times smaller than the corresponding parameter estimates. The average vol-

**TABLE 3**  
Pharmacokinetic Parameter Estimates Based on a Five-Compartment Model Fit to Blood, Urine and Imaging Data from Clinical Diagnostic Studies Involving cT84.66 Labeled with Indium-111

Kinetic parameter estimate (s.d.)*	Patient no.									Mean†	s.e.‡
	7	8	10	11	13	14	15	17	18		
$k_{bl}$ (blood to liver; $hr^{-1}$ )	0.014 (0.003)	0.006 (0.001)	0.005 (0.001)	0.009 (0.002)	0.062 (0.014)	0.003 (0.001)	0.046 (0.011)	0.008 (0.002)	0.005 (0.001)	0.017 (0.004)§	0.007
$k_{lb}$ (liver to blood; $hr^{-1}$ )	0.011 (0.008)	0.002 (0.005)	0.008 (0.008)	0.030 (0.014)	0.012 (0.010)	0.007 (0.007)	0.017 (0.012)	0.015 (0.008)	0.020 (0.010)	0.013 (0.009)	0.003
$k_{br}$ (blood to residual; $hr^{-1}$ )	0.027 (0.008)	0.025 (0.007)	0.023 (0.005)	0.027 (0.008)	0.047 (0.011)	0.005 (0.001)	0.037 (0.008)	0.019 (0.005)	0.036 (0.035)	0.027 (0.010)	0.004
$k_{rb}$ (residual to blood; $hr^{-1}$ )	0.022 (0.014)	0.032 (0.015)	0.022 (0.010)	0.039 (0.018)	0.000 (0.007)	0.002 (0.007)	0.000 (0.009)	0.019 (0.012)	0.115 (0.127)	0.028 (0.024)	0.012
$K_{lu}$ (liver to urine; $hr^{-1}$ )	0.005 (0.001)	0.006 (0.001)	0.008 (0.001)	0.008 (0.001)	0.005 (0.001)	0.008 (0.001)	0.005 (0.001)	0.005 (0.001)	0.009 (0.001)	0.007 (0.001)	0.001
$k_{rf}$ (residual to feces; $hr^{-1}$ )	0.002 (0.001)	0.004 (0.001)	0.004 (0.001)	0.004 (0.001)	0.008 (0.006)	0.008 (0.002)	0.017 (0.003)	0.005 (0.001)	0.008 (0.003)	0.007 (0.002)	0.002
Volume (liters)	8.493 (0.224)	5.222 (0.126)	4.956 (0.081)	4.413 (0.092)	3.849 (0.157)	4.025 (0.067)	4.816 (0.169)	5.062 (0.138)	7.382 (0.396)	5.358 (0.161)	0.520
Fraction blood in liver ( $f_{bl}$ )	0.241 (0.002)	0.146 (0.008)	0.142 (0.004)	0.131 (0.010)	0.184 (0.041)	0.132 (0.011)	0.210 (0.032)	0.216 (0.001)	0.133 (0.010)	0.171 (0.013)	0.014

\*Parameter estimates and corresponding s.d. obtained using ordinary least squares fit to each patient's data as a function of time.

†Mean parameter estimates obtained by averaging across the nine patients.

‡s.e. of the mean parameter estimates.

§Average s.d. obtained by averaging across the nine patients.

**TABLE 4**  
Area under the Curve and R<sup>2</sup> Estimates for Models 3C and 5C

Data source	Model	Statistic	Patient no.															
			1	2	3	4	5	6	7	8	10	11	13	14	15	17	18	
Blood	3C	R <sup>2</sup>	0.99	0.99	0.99	0.81	1.00	0.99	0.99	0.99	1.00	1.00	1.00	1.00	0.99	0.99	1.00	
		AUC*	0.52	6.81	5.63	1.71	3.27	8.70	3.73	8.59	8.57	10.76	2.19	15.04	2.69	8.68	6.07	
	5C	R <sup>2</sup>	NA	NA	NA	NA	NA	NA	0.99	0.99	1.00	0.99	1.00	1.00	0.99	0.99	0.99	
Urine	3C	AUC*	NA	NA	NA	NA	NA	NA	4.22	8.41	9.14	11.04	2.85	14.98	3.05	8.69	7.73	
		R <sup>2</sup>	0.94	0.99	0.93	0.80	0.95	0.97	0.94	1.00	0.97	0.88	0.78	0.87	0.52	0.68	0.99	
	5C	R <sup>2</sup>	NA	NA	NA	NA	NA	NA	0.92	0.99	0.95	0.90	0.86	0.96	0.81	0.76	0.96	
Liver	3C	AUC	NA	NA	NA	NA	NA	NA	8.91	7.99	6.10	6.58	12.55	5.26	9.78	5.44	6.64	
		R <sup>2</sup>	NA	NA	NA	NA	NA	NA	1.00	0.97	1.00	1.00	1.00	1.00	0.99	1.00	1.00	
	5C	AUC	NA	NA	NA	NA	NA	NA	27.94	19.48	14.66	15.45	26.75	14.57	24.32	21.63	15.01	
Whole body	5C	R <sup>2</sup>	NA	NA	NA	NA	NA	NA	1.00	1.00	1.00	1.00	1.00	1.00	1.00	1.00	1.00	
		AUC	NA	NA	NA	NA	NA	NA	NA	83.84	81.09	81.86	82.99	63.33	81.75	55.45	80.11	79.86

\*Units for area under the curve (AUC), mCi/hr.  
NA = not applicable.

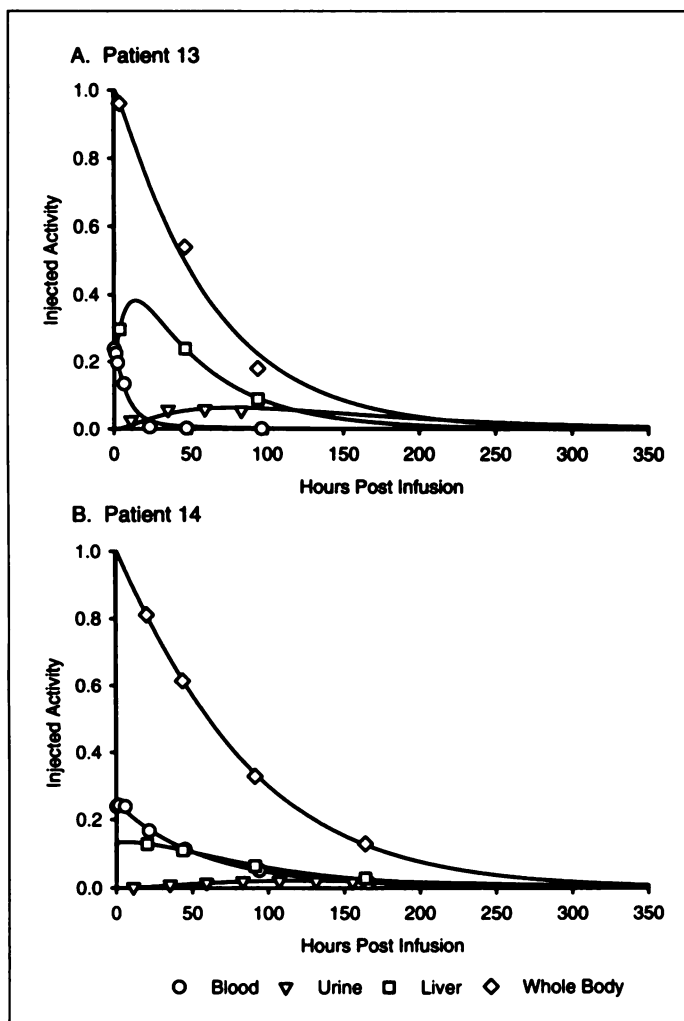


**FIGURE 3.** (A) Activity data and model 5C-derived curves for Patient 13. Time is measured in hr postinfusion of <sup>111</sup>In-cT84.66. This patient was characterized by relatively fast clearance of the chimeric MAb from the blood. Data were obtained from whole body and liver (plus hepatic blood) images, as well as from blood samples and collected urine. Urine data were measured as total accumulation of activity. (B) Model 5C-derived curves and data for Patient 14. This patient was characterized by a relatively slow clearance of the MAb. Clearance from blood took approximately five times longer than for Patient 13.

ume of the blood distribution compartment using model 3C was 5.83 (range, 3.82–8.65). Model 5C described the data from the subcohort very well, as evidenced by the small s.d. relative to the corresponding parameter estimates and the large R<sup>2</sup> statistics (median = 0.92; range, 0.76–1.00); s.d. for the estimates of V and f<sub>b1</sub> using either model were smaller than the corresponding parameter estimates by an order of magnitude or more in all cases. The average volume of the blood distribution compartment using model 5C was 5.36 liters (range 3.85–8.49 liters), average f<sub>b1</sub> was 0.17 (range 0.13–0.24). For 63 of the 72 parameters estimated (8 parameters per patient), the s.d. were between 2–8 times smaller than the corresponding PK parameter estimates. Comparing the R<sup>2</sup> statistics for blood and urine between models 3C and 5C, both models fit the blood data exceptionally well (range 0.99–1.00 under both models). Model 5C fit the urine data better than did model 3C for five of the nine patients, and both models fit the data well for the remaining four. Model 5C also fit the liver and whole-body data exceptionally well, with R<sup>2</sup> equal to 1.00 for the whole-body data and ranging from 0.97 to 1.00 for liver.

Figure 3 includes the observed blood, urine, liver and whole-body biodistribution results and modeled curves (model 5C) for two representative patients (Patients 13 and 14). These patients were chosen for their relatively rapid and slow MAb clearance from the blood, respectively. In both cases, model 5C accurately described patient data from the several organ systems. The uptake units are in percent IA.

The <sup>111</sup>In-cT84.66 and projected <sup>90</sup>Y-cT84.66 absorbed dose estimates on a per-mCi basis to 13 target organs are shown in Table 5 for the subcohort (model 5C only). These organs were selected for inclusion on the basis of either their relatively large dose estimates or their genetic significance (ovaries, testes and whole body). On the average, the highest estimated <sup>111</sup>In-cT84.66 doses were administered to the liver (mean ± s.e. 3.18 ± 0.25 rad/mCi; range 2.09–4.44 rad/mCi), followed by the wall of the gallbladder (mean ± s.e. 1.20 ± 0.05 rad/mCi; range 0.94–1.40 rad/mCi). The average <sup>111</sup>In-cT84.66 dose ± s.e. to the red marrow was 0.55 ± 0.04 rad/mCi, ranging from 0.34 to 0.74 rad/mCi. The average <sup>111</sup>In-T84.66 dose ± s.e. to the whole body was 0.51 ± 0.02 rad/mCi, ranging from 0.41 to 0.58 rad/mCi. For <sup>90</sup>Y-cT84.66, the highest estimated doses were administered to the liver (mean ± s.e. 24.78 ± 2.38 rad/mCi; range 15.02–37.07 rad/mCi), followed by the spleen (mean ± s.e. 4.50 ± 0.98 rad/mCi; range 1.07–10.20 rad/mCi)

**TABLE 5**  
Indium-111 and Yttrium-90 cT84.66 Antibody Absorbed Dose Estimates (rad/mCi)\*

Target organ	Label	Patient no.									Mean <sup>†</sup>	s.e. <sup>‡</sup>
		7	8	10	11	13	14	15	17	18		
Adrenals	<sup>111</sup> In	0.89	0.95	0.87	0.89	0.87	0.89	0.77	0.81	0.71	0.85	0.02
	<sup>90</sup> Y	1.42	2.01	2.25	2.23	1.27	2.08	1.07	1.42	1.64	1.71	0.15
Bone surfaces	<sup>111</sup> In	0.64	0.79	0.83	0.87	0.53	0.90	0.47	0.67	0.72	0.71	0.05
	<sup>90</sup> Y	2.09	2.76	3.00	3.37	1.25	4.00	1.33	2.87	3.21	2.65	0.31
Gallbladder wall	<sup>111</sup> In	1.35	1.29	1.13	1.16	1.40	1.12	1.26	1.14	0.94	1.20	0.05
	<sup>90</sup> Y	1.42	2.01	2.25	2.23	1.27	2.08	1.07	1.42	1.64	1.71	0.15
Heart wall	<sup>111</sup> In	0.76	1.04	0.76	0.87	0.69	1.29	0.57	0.88	0.57	0.83	0.08
	<sup>90</sup> Y	2.79	4.85	2.56	3.49	1.83	7.63	1.21	4.50	1.78	3.41	0.67
Kidneys	<sup>111</sup> In	0.94	0.98	0.73	0.73	0.65	0.91	0.58	0.95	0.61	0.79	0.05
	<sup>90</sup> Y	4.48	4.62	2.25	2.23	1.27	4.52	1.07	5.34	1.78	3.06	0.55
Liver	<sup>111</sup> In	3.70	3.39	2.63	2.76	4.44	2.63	4.03	2.92	2.09	3.18	0.25
	<sup>90</sup> Y	27.93	26.45	20.02	21.10	37.07	19.94	33.73	21.71	15.02	24.78	2.38
Lungs	<sup>111</sup> In	0.55	0.69	0.66	0.68	0.58	0.69	0.50	0.52	0.49	0.60	0.03
	<sup>90</sup> Y	1.42	2.01	2.25	2.23	1.27	2.08	1.07	1.42	1.64	1.71	0.15
Ovaries	<sup>111</sup> In	NA	0.58	0.63	0.64	0.39	0.62	0.33	NA	NA	0.53	0.05
	<sup>90</sup> Y	NA	2.01	2.25	2.23	1.27	2.08	1.07	NA	NA	1.82	0.21
Pancreas	<sup>111</sup> In	0.84	0.95	0.88	0.88	0.83	0.88	0.74	0.78	0.69	0.83	0.03
	<sup>90</sup> Y	1.42	2.01	2.25	2.23	1.27	2.08	1.07	1.41	1.64	1.71	0.15
Red marrow	<sup>111</sup> In	0.49	0.59	0.61	0.66	0.36	0.74	0.34	0.56	0.59	0.55	0.04
	<sup>90</sup> Y	2.48	3.37	3.60	4.29	1.24	5.55	1.55	3.72	4.12	3.32	0.46
Spleen	<sup>111</sup> In	0.74	1.27	0.94	0.60	0.41	0.76	0.35	0.91	0.66	0.74	0.09
	<sup>90</sup> Y	4.69	10.20	6.25	2.23	1.27	4.14	1.07	6.77	3.90	4.50	0.98
Testes	<sup>111</sup> In	0.29	NA	NA	NA	NA	NA	NA	0.29	0.34	0.31	0.01
	<sup>90</sup> Y	1.42	NA	NA	NA	NA	NA	NA	1.42	1.64	1.49	0.07
Total body	<sup>111</sup> In	0.49	0.57	0.57	0.58	0.46	0.57	0.41	0.46	0.46	0.51	0.02
	<sup>90</sup> Y	2.17	2.71	2.76	2.78	2.15	2.71	1.89	2.06	2.08	2.37	0.12

\*Each patient received 5mCi.

<sup>†</sup>Mean dose obtained by averaging across the 9 patients.

<sup>‡</sup>s.e. of the mean dose.

NA = not applicable.

and the red marrow (mean  $\pm$  s.e.  $3.32 \pm 0.46$  rad/mCi; range 1.24–5.55 rad/mCi). The average <sup>90</sup>Y-cT84.66 dose estimate to the whole body was  $2.377 \pm 0.12$  rad/mCi, ranging from 1.89 to 2.78 rad/mCi. Indium-111-cT84.66 and projected <sup>90</sup>Y-cT84.66 doses administered to the testes and ovaries were relatively small. Absorbed dose estimates for the target organs included as output from the MIRDOSE3 program that are not reported in Table 5 can be obtained from the authors.

Based on the clinician's assessment of the antibody scans, five patients cleared the MAb from the blood quickly (Patients 1, 4, 5, 13 and 15). These five patients also had the smallest values for the blood AUCs and the largest values for the urine AUCs (Table 4). Patient 14 cleared the antibody most slowly and was found to have a large value for the blood AUC and a small value for the urine AUC. For Patients 13 and 15, the  $k_{tb}$  estimates were close to zero and the  $k_{bl}$  estimates were largest. Urine AUCs based on models 5C and 3C were 12.55 and 16.42 mCi-hr for Patient 13 and 9.78 and 12.24 mCi-hr for Patient 15, respectively. The AUCs for the two models were similar for the other seven patients in the subcohort.

## DISCUSSION

Variations of model 5C, which incorporated the kidney data and which connected urine and feces to the residual compartment, were examined. Model 5C was the most robust in its application to all patients with digital imaging data. Kinetic parameter estimates were stable, as evidenced by the small s.e. for these estimates and the large  $R^2$  values. A variation of model 3C, which connected the urine compartment to the blood

instead of the residual compartment, was also examined but was found to be less robust.

Because the primary toxicity from <sup>90</sup>Y-cT84.66 therapy is likely to be hematopoietic, planned future therapy trials will involve stem cell support, such that estimation of doses to secondary organs becomes very important. Modeling the digital imaging and urine data in addition to the blood uptake provides a method for obtaining reliable dose estimates for the secondary organs that correctly uses the maximum amount of information available. Because the fits to these data are as good or better than the fits to the simpler model (model 3C), the dosimetry results based on model 5C are preferable.

Methods used here required certain assumptions about the data and methods. First, to estimate the <sup>90</sup>Y-cT84.66 absorbed dose estimates, AUCs for the <sup>90</sup>Y-MAB were obtained by exchanging the physical decay constant of <sup>111</sup>In with that of <sup>90</sup>Y in the modeling equations. This approach requires an explicit assumption that the biodistribution and, hence, modeling parameters will not have been affected by the nature of the radiolabel. Animal studies published by this group (27) have shown that the biodistribution of this antibody is only slightly changed by the nature of the radiolabel, so this extrapolation of these results to human studies seems reasonable. The second assumption relates to the completeness of the urine data. Because the patients collected their own urine in an unsupervised manner, it is possible that using these data to examine urinary clearance may be unreliable. Nonetheless, we found the urine data to be very useful in explaining the clearance characteristics of <sup>111</sup>In-MAB. Model 5C fit the urine data well,

providing us with the best available estimates for urine clearance kinetics. Although the last urine collection was before the last scan time, curves of the cumulative percent IA activity in the urine suggest that very little additional urine activity would have been found in the urine after 60 hr.

We compared our model to one in which the liver compartment was linked to the fecal compartment and the urine compartment linked to the central compartment (not shown). However, the imaging study results suggested that the fecal route of elimination of antibody was through the wall of the gut and not through the liver. A model including the feces compartment directly off a nonhepatic tissue compartment (residual) characterized the data better than the model with the feces linked to the liver. Our modeling results of the blood and urine data were consistent with HPLC analysis of the blood and urine, which showed that radioactive species in the urine had a much lower molecular weight than that found in the blood. Therefore, the majority of the activity that appeared in the urine was presumed to be a metabolic product from the liver, which cleared the kidney with first-pass kinetics. The majority of the activity that appeared in the blood was found to be intact antibody (16).

As we have shown previously (19), the inclusion of decay in the modeling equations is important because it allows the user to model the data as acquired rather than as artificially corrected for decay. If weighted least squares regression is performed, modeling the data expressed as fractional IA will produce different results than if the data are expressed as fractional injected dose because the weighting schemes examined involve the observed data. For this study, the data were expressed as IA. Although the best fits to the data were obtained using ordinary least squares, examination of different weighting schemes is important. We recommend trying a weighting approach in which a variance model for each data source is specified and maximum likelihood estimation is then used to estimate the variance parameters.

We are not aware of any published results of studies reporting absorbed doses for  $^{90}\text{Y}$ -MAbs. The results from this trial suggest that the largest projected  $^{90}\text{Y}$ -cT84.66 absorbed dose estimate was delivered to the liver (24.775 rad/mCi), followed by the spleen (4.500 rad/mCi) and the red marrow (3.324 rad/mCi). However, there are previous results reported for absorbed dose estimates using  $^{111}\text{In}$ -MAbs, which are consistent with the absorbed dose estimates made herein. Taylor et al. (28) estimated liver doses of 1.62 rad/mCi for the antibody ZME018. Similarly, Buijs et al. (29) and Fairweather et al. (30) reported hepatic estimates of 3.18 and 2.90 rad/mCi for  $\text{F(ab')}_2$  ovarian and anti-CEA antibodies, respectively. The latter two values were in very close agreement with our estimate of 3.18 rad/mCi (Table 3). Our whole-body estimate of 0.51 rad/mCi was quite comparable to the values of 0.54 and 0.50 rad/mCi reported by Taylor et al. (28) and Fairweather et al. (30), respectively. Our estimated splenic (0.74 rad/mCi), kidneys (0.79 rad/mCi) and red marrow (0.55 rad/mCi) doses were lower than the two other literature values by a factor of two or more. Taylor et al. (28) documented splenic estimates of 4.72 rad/mCi; Buijs et al. (29) reported 5.37 rad/mCi. The same groups gave kidney estimates of 1.94 and 4.37 rad/mCi, respectively, with marrow estimates in the range of 0.9–1.9 rad/mCi. However, because of the different antibody types (28), fragment mass (29) and chelation chemistry, it is difficult to compare their results in every organ directly to ours. Fairweather et al. (30), who used an antibody type similar to cT84.66, reported absorbed dose estimates for two organs only,

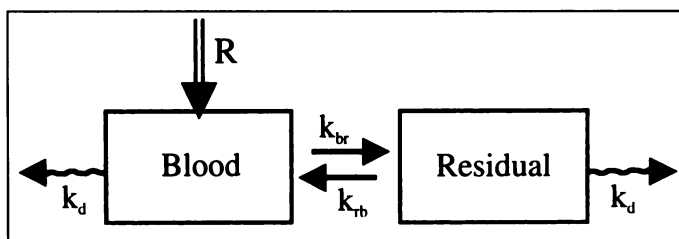


FIGURE 4. Two-compartment model used to fit the blood data for the purpose of determining the optimal specimen collection times for future patients.

liver and whole body; these were in agreement with the results reported here.

Several previous mathematical models have been developed to describe the human biodistribution of radiolabeled antibodies. None of the models used in these earlier representations are comparable to the models presented here. We do not know of any closed multicompartment model involving a chimeric antibody (9,10). Additionally, both Koizumi et al. (12) and Eger et al. (31) required the assumption of saturable compartments to describe the data from their antibody trials.

Norrgrén et al. (32) have reported rate constants from a study using murine MAbs in nude rats. Their model was similar to model 5C in that it featured a mammillary representation with several organs being in contact with the blood. They estimated a  $k_{bl}$  of  $0.015 \text{ hr}^{-1}$  and a  $k_{lb}$  of  $0.12 \text{ hr}^{-1}$ , compared to our results of  $0.017 \text{ hr}^{-1}$  and  $0.027 \text{ hr}^{-1}$ , respectively. Aside from species differences, the disparity between the values for  $k_{lb}$  could be due to the fact that their antibody was labeled with a radioiodine.

A subroutine of the ADAPT II, SAMPLE, performs an optimal sampling sequential estimation procedure using parameter estimates from previous subjects in the group to determine the optimal sampling times for patients accrued to future trials involving the cT84.66 antibody (33). To provide more informative PK results, after the first 12 patients were accrued to the trial, SAMPLE was used to determine the optimal times for blood collections to be used for the remaining three patients to be accrued to this trial. A two-compartment model shown in Figure 4 was fit to each of the 12 patients' blood data only. The resultant optimal sampling times tended to cluster into two patterns, corresponding to how quickly the patient cleared the antibody from the blood. A final set of blood draw collection time points was established, such that knowledge of a patient's antibody clearance characteristics was not required at the start of the patient's infusion. These values were: preinfusion, at the start of infusion ( $t = 0$ ) and at approximately 4, 16, 36, 48, 108, 168 and 500 hr postinfusion. The final set of blood collection times was chosen so that:

1. The times would be convenient for the hospital's staffing schedules and the patients' schedules; and
2. The collection times would not depend on prior knowledge of the patient's antibody clearance characteristics.

The latter condition existed because of the indeterminacy of clearance status until after the first scan. Although the SAMPLE subroutine recommended only four optimal time points for blood draws, seven optimal time points were selected to accommodate the considerations mentioned above and to account for anticipated interpatient variability observed as larger numbers of patients are examined. We found that obtaining a sample at or beyond the half-life of the antibody is important for the model to accurately fit the data in the tail of the blood curve. For the trial reported here, the collection time for the last blood

sample was limited by whether the patient was scheduled to undergo surgery.

The SAMPLE subroutine could also be used to identify optimal imaging times. However, the model required would necessarily be much more complex than the two-compartment model specified for the blood data (Fig. 4). At the time of the SAMPLE analysis of the blood data, digital imaging data were available for only a very small subset of patients. With complete data available for the subcohort, plans to perform a SAMPLE analysis of these data are underway.

Finally, we should mention that methods for obtaining population PK estimates exist which, with a larger sample size, may provide a better representation of the patient datasets. To this end, we have begun exploring the use of a software program called IT2S (Iterative Two-Stage), which runs under ADAPT II (unsupported research tool, Collins D and Forrest A, State University of New York, Buffalo, NY, 1997.) This program uses an iterative approach involving the MAP (maximum a posterior) Bayesian estimator and a generalized least-squares type of algorithm to update the error variance model. The IT2S strategy has been shown to perform better than the single-iteration, generalized least-squares approach and may be useful in the area of radioimmunotherapy for several reasons. First, the fit to a patient's data is guided by what has been observed in the population. This is important given the limited amount of data available and the potential for error associated with a specific time point. The ultimate reason for modeling data from a pretherapy <sup>111</sup>In antibody infusion is to obtain information enabling the clinician to augment the therapy plan if the dose level to any organ is suboptimal. Second, as we gain additional experience with the kinetic modeling of data from a larger number of patients, we will be interested in potentially reducing the amount of data required for these trials by performing limited sampling analyses.

## CONCLUSION

A three-compartment model was successfully used to represent blood and urine chimeric anti-CEA antibody data from 15 cancer patients, and a five-compartment model was successfully used to represent imaging, blood and urine data from a subcohort of these patients, as evidenced by the small s.e. for the kinetic parameter estimates and R<sup>2</sup> statistics. Modeling the digital imaging data in addition to the urine and blood uptake provides a method for obtaining reliable dose estimates for the secondary organs that correctly uses the maximum amount of information available. Through modeling, the AUC of activity against time was determined and used in the estimation of the absorbed radiation doses to normal organs and tissues. In future therapy trials, these results will be used to guide the treatment plan.

## ACKNOWLEDGMENTS

We thank Lupe Ettinger, RN (protocol nurse); Gina Farino, BS (data manager); James Kao, MS, and Randal Woo, MS (radio-pharmacy); Kathleen Thomas, CNMT, Ron Fomin, CNMT, and Joy Bright, CNMT (nuclear medicine); Karla Carlson (graphics); and Edward Newman, PhD, and Timothy Synold, PharmD, for their contributions. This work was supported in part by funds from the National Institutes of Health Cancer Center Core Grant 33527 and Grants PO143904 and RO142329.

## REFERENCES

1. Murray JL, Rosenblum MG, Sobel RE, et al. Radioimmunoimaging in malignant melanoma with <sup>111</sup>In-labeled monoclonal antibody 96.5. *Cancer Res* 1985;45:2376-2381.

2. Stewart JS, Hird V, Snook D, et al. Intraperitoneal <sup>131</sup>I and <sup>90</sup>Y labeled monoclonal antibodies for ovarian cancer: pharmacokinetics and normal tissue dosimetry. *Int J Cancer* 1988;3(suppl):71-76.
3. Corbisiero RM, Yamauchi DM, Williams LE, et al. Comparison of immunoscintigraphy and computerized tomography in identifying colorectal cancer: individual lesion analysis. *Cancer Res* 1991;51:5704-5711.
4. Vriesendorp HM, Herpst JM, Lechner PK, et al. Polyclonal yttrium-90 labeled antifermitin for refractory Hodgkin's disease. *Int J Radiat Oncol Biol Phys* 1989;17:815-821.
5. Press OW, Early JF, Badger CC, et al. Treatment of refractory non-Hodkin's lymphoma with radiolabeled MB-1 (anti-CD37) antibody. *J Clin Oncol* 1989;7:1027-1038.
6. DeNardo SJ, Mirick GR, Kroger LA, et al. The biologic window for chimeric L6 radioimmunotherapy. *Cancer* 1994;73(suppl):1023-1032.
7. Schroff RW, Foon KA, Beatty SM, Oldham RK, Morgan AC. Human antimurine immunoglobulin responses in patients receiving monoclonal antibody therapy. *Cancer Res* 1985;45:879-885.
8. Beatty JD, Duda RB, Williams LE, et al. Preoperative imaging of colorectal carcinoma with <sup>111</sup>In-labeled anti-carcinoembryonic antigen monoclonal antibody. *Cancer Res* 1986;46:6494-6502.
9. Meredith RF, LoBuglio AF, Plott WE, et al. Pharmacokinetics, immune response, and biodistribution of iodine-131-labeled chimeric mouse/human IgG1 k17-1A monoclonal antibody. *J Nucl Med* 1991;32:1162-1168.
10. Khazaeli MB, Saleh MN, Liu TP, et al. Pharmacokinetics and immune response of <sup>131</sup>I-chimeric mouse/human B7.2.3 (human g4) monoclonal antibody in humans. *Cancer Res* 1991;51:5461-5466.
11. Foster DM, Boston RC. The use of computers in compartmental analysis: the SAAM and CONSAM programs. In: Robertson JS, ed. *Compartment distribution of radio-tracers*. Boca Raton, FL: CRC Press; 1983:73-81.
12. Koizumi K, DeNardo GL, DeNardo SJ, et al. Multicompartment analysis of the kinetics of radioiodinated monoclonal antibody in patients with cancer. *J Nucl Med* 1986;27:1243-1254.
13. Shively JE, Beatty JD. CEA-related antigens: molecular biology and clinical significance. *Crit Rev Oncol Hematol* 1985;2:355-399.
14. Krishnamurthy S, Morris JF, Antonovic R, et al. Evaluation of primary lung cancer with indium-111 anticarcinoembryonic antigen (type ZCE025) monoclonal antibody scintigraphy. *Cancer* 1990;65:458-465.
15. Esteban JM, Raubitschek AA, Felder B, Williams LE, Wong JYC, Shively JE. Breast tumor xenograft targeting and therapy trials using radiolabeled chimeric anti-CEA monoclonal antibody T84.66. *Oncol Rep* 1995;2:237-242.
16. Wong JYC, Thomas GE, Yamauchi D, et al. Clinical evaluation of an <sup>111</sup>In-labeled anti-CEA monoclonal antibody. *J Nucl Med* 1997;38:1951-1959.
17. D'Argenio DZ, Schumitzky A. A program package for simulation and parameter estimation in pharmacokinetic systems. *Comput Prog Biomed* 1979;9:115-134.
18. Yamaoka K, Nakagawa T, Uno T. Application of Akaike's information criterion (AIC) in the evaluation of linear pharmacokinetic equations. *J Pharmacokin Biopharm* 1978;6:165-175.
19. Williams LE, Odom-Maryon TL, Liu A, et al. On the correction for radioactive decay in pharmacokinetic modeling. *Med Phys* 1995;22:1619-1626.
20. Thomas SR, Maxon HR, Kereiakes JG. In vivo quantitation of lesion radioactivity using external counting methods. *Med Phys* 1976;3:253-255.
21. Giltinan DM, and Ruppert D. Fitting heteroscedastic regression models to individual pharmacokinetic data using standard statistical software. *J Pharmacokin Biopharm* 1989;17:601-615.
22. Loevinger R, Berman M. A revised schema for calculation of the absorbed dose from biologically distributed radionuclides, MIRD Pamphlet No. 1, Revised. New York: Society of Nuclear Medicine; 1976.
23. Stabin MG. MIRDose: Personal computer software for internal dose assessment in nuclear medicine. *J Nucl Med* 1996;37:538-546.
24. Siegel JA, Wessels BW, Watson EE, et al. Bone marrow dosimetry and toxicity for radioimmunotherapy. *Anti Immunoconjug Radiopharm* 1990;3:213-233.
25. Guyton AC. *Textbook of medical physiology*, 5th Ed. Philadelphia: W. B. Saunders Company; 1976:426-428.
26. Williams LE, Ettinger LM, Cofresi E, Raubitschek AA, Wong JYC. A shielded, automated injector for energetic beta-emitting radionuclides. *J Nucl Med Technol* 1995;23:29-32.
27. Williams LE, Primus FJ, Wong JYC. Biodistribution of an In-111 or Y-90 labeled chimeric anti-CEA monoclonal antibody (cT84.66) following its large scale production in a bioreactor. *Tumor Targeting* 1996;2:116-124.
28. Taylor A, Milton W, Eyre H, et al. Radioimmunodetection of human melanoma with indium-111-labeled monoclonal antibody. *J Nucl Med* 1988;29:329-337.
29. Buijs WCAM, Massuger LFAG, Claessens RAMJ, Kenemans P, Corstens FHM. Dosimetric evaluation of immunoscintigraphy using indium-111-labeled monoclonal antibody fragments in patients with ovarian cancer. *J Nucl Med* 1992;33:1113-1120.
30. Fairweather DS, Bradwell AR, Dykes PW, Vaughan AT, Watson-James SF, Chandler S. Improved tumor localization using indium-111-labeled antibodies. *Br Med J* 1983;287:167-170.
31. Eger RR, Covell DG, Carrasquillo J, et al. Kinetic model for the biodistribution of an <sup>111</sup>In-labeled monoclonal antibody in humans. *Cancer Res* 1987;47:3328-3336.
32. Norrgren K, Strand SE, Ingvar C. Contrast enhancement in RIT and modification of the therapeutic ratio in RIT: a theoretical evaluation of simulated extracorporeal immunoabsorption. *Antibody Immunoconjug Radiopharm* 1992;5:61-73.
33. D'Argenio DZ. Optimal sampling times for pharmacokinetic experiments. *J Pharmacokin Biopharm* 1978;9:739-756.